Published for SISSA by Springer

Received: November 13, 2016
Accepted: December 29, 2016
Published: January 5, 2017

Heavy Higgs bosons at low $\tan\beta$: from the LHC to 100 TeV

Nathaniel Craig,[a] **Jan Hajer,**[b,c] **Ying-Ying Li,**[b] **Tao Liu**[b] **and Hao Zhang**[a]

[a] *Department of Physics, University of California, Santa Barbara, CA 93106, U.S.A.*

[b] *Department of Physics, The Hong Kong University of Science and Technology, Clear Water Bay, Kowloon, Hong Kong S.A.R., P.R.C.*

[c] *Institute for Advanced Study, The Hong Kong University of Science and Technology, Clear Water Bay, Kowloon, Hong Kong S.A.R., P.R.C.*

E-mail: ncraig@physics.ucsb.edu, jan.hajer@ust.hk, ylict@connect.ust.hk, taoliu@ust.hk, zhanghao@physics.ucsb.edu

Abstract: We present strategies to search for heavy neutral Higgs bosons decaying to top quark pairs, as often occurs at low $\tan\beta$ in type II two Higgs doublet models such as the Higgs sector of the MSSM. The resonant production channel is unsatisfactory due to interference with the SM background. We instead propose to utilize same-sign dilepton signatures arising from the production of heavy Higgs bosons in association with one or two top quarks and subsequent decay to a top pair. We find that for heavier neutral Higgs bosons the production in association with one top quark provides greater sensitivity than production in association with two top quarks. We obtain current limits at the LHC using Run I data at 8 TeV and forecast the sensitivity of a dedicated analysis during Run II at 14 TeV. Then we perform a detailed BDT study for the 14 TeV LHC and a future 100 TeV collider.

Keywords: Beyond Standard Model, Higgs Physics

ArXiv ePrint: 1605.08744

doi:10.1007/JHEP01(2017)018

JHEP01(2017)018

Contents

JHEP01(2017)018

1 Introduction

The search for additional Higgs bosons is a high priority for current and future colliders. The ATLAS and CMS collaborations have performed searches for heavy neutral [1–9] and charged [10–12] Higgs bosons during the first run of the Large Hadron Collider (LHC) at $\sqrt{s} = 8\,\text{TeV}$. The reach of such searches will expand considerably in the future; in its second run, the LHC has started to take data at $\sqrt{s} = 13\,\text{TeV}$, with an eventual goal of collisions at $\sqrt{s} = 14\,\text{TeV}$. In the long run, the center-of-mass energy of next-generation pp-colliders can be as much as an order of magnitude higher than that of the LHC. Such a high energy scale opens up new signal channels which are suppressed at lower energies.

Among the most challenging scenarios are those in which heavy neutral Higgs bosons decay predominantly into $t\bar{t}$ pairs. Dedicated studies probing the heavy Higgs sector via $t\bar{t}$ final states have recently been presented for the LHC [13–17] and a 100 TeV collider [15]. In motivated models for extended Higgs sectors described by a type II two Higgs doublet model (2HDM), the moderate $\tan\beta$ region can be covered up to 1 TeV using BDT methods, in large part by using bottom quark associated production. However, the low $\tan\beta$ region

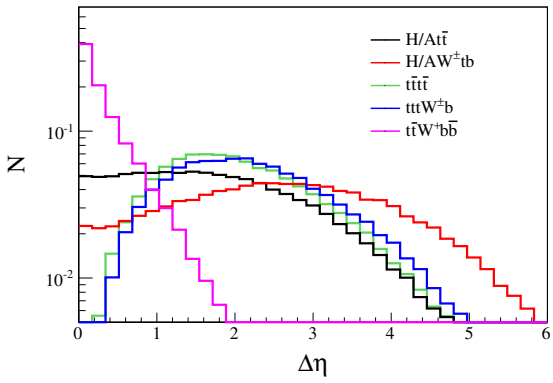

(a) 500 GeV heavy Higgs at 14 TeV.

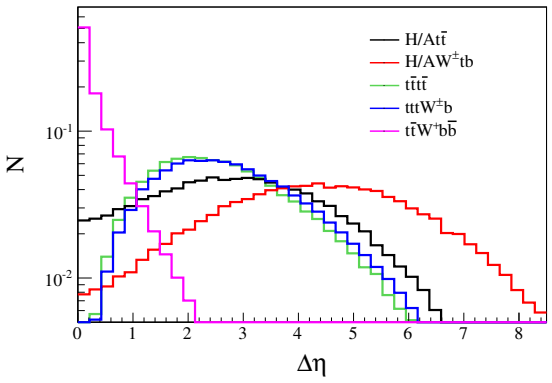

(b) 5 TeV heavy Higgs at 100 TeV.

Figure 1. (a) Distribution of the rapidity difference between two bottom quarks at 14 TeV for a 500 GeV heavy Higgs. The rapidity difference is calculated between the bottom pair found in the decay products of the particles produced in association with the heavy Higgs, which involves either one (red) or two (black) top quarks. (b) Distribution of the rapidity difference at 100 TeV for a 5 TeV heavy Higgs. For comparison, in each case we also show the maximal rapidity difference between all b-quarks in the $t\bar{t}t\bar{t}$ background (green), as well as between the soft additional b and one of the b-quarks coming from a top decay in the $tttW^{\pm}b$ background (blue). Additionally, we show the rapidity difference between the two b quarks in the $t\bar{t}W^{\pm}b\bar{b}$ background (pink).

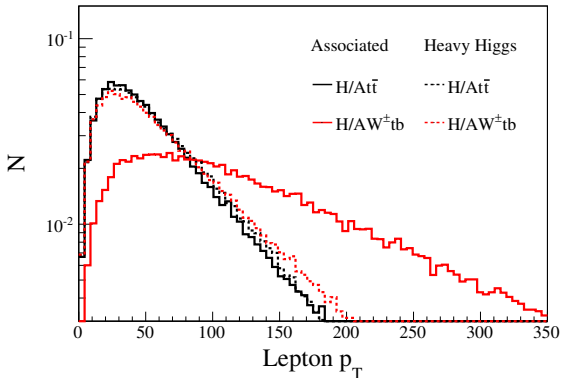

(a) 500 GeV heavy Higgs at 14 TeV.

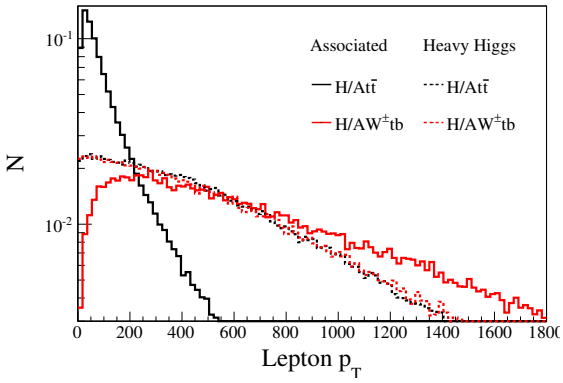

(b) 5 TeV heavy Higgs at 100 TeV.

Figure 2. (a) Transverse momenta of the leptons at 14 TeV for a 500 GeV heavy Higgs. The transverse momenta are plotted for the two signal channels $H/At\bar{t}$ (black) and $H/AW^{\pm}tb$ (red) for cases in which the lepton comes from the decay products of a heavy Higgs boson (dotted) or the decay products of an associated particle (W boson for three-top case) (solid). (b) Transverse momenta of the leptons at 100 TeV for a 5 TeV heavy Higgs.

remains thus far uncovered as the conventional resonant $t\bar{t}$ channel suffers from interference with the Standard Model background [18–21] and the cross section for bottom quark associated production is negligible. This motivates dedicated searches for signals in the low $\tan\beta$ region; the development of strategies for such searches is the goal of this paper.

Given that gluon fusion and bottom quark associated production modes are unpromising, we propose to cover the low $\tan\beta$ region through top associated production modes,

JHEP01(2017)018

namely the channels

- $pp \to t\bar{t}H \to t\bar{t}t\bar{t}$,
- $pp \to \bar{t}HW^+b \to \bar{t}t\bar{t}W^+b$ and $pp \to tHW^-\bar{b} \to tt\bar{t}W^-\bar{b}$.[1]

These channels are ideally suited for probing the low $\tan\beta$ region, since they do not suffer significant interference with Standard Model backgrounds, and the corresponding production cross sections are maximized for low $\tan\beta$ in type II 2HDM. Various aspects of these channels have already been discussed [22–25]. In this work we develop an optimized strategy for probing extended Higgs sectors in top associated production by focusing on the three main kinematic features of these channels: first, large heavy Higgs masses lead to a sizable scalar sum of transverse momenta H_T. Second, we use the forward-/backwardness of the accompanying quarks. Although the heavy Higgs is produced in association with one or two top quarks, the bottom quarks resulting from heavy Higgs decays still tend to be forward/backward, as shown in figure 1. This feature discriminates against backgrounds other than the irreducible $t\bar{t}t\bar{t}$ background. Third, we make use of the same-sign di-lepton (SSDL) signature present in these signal channels. Especially in the $pp \to \bar{t}HW^+b$ channel, the transverse momentum of the lepton originating from the decay of the associated W boson is comparable to the one originating from the decay of the heavy Higgs, as shown in figure 2.

The paper is organized as follows: in section 2, we study general features of heavy Higgs associated production at the Large Hadron Collider and a future pp-collider operating at $\sqrt{s} = 100\,\text{TeV}$. We then consider constraints from existing SSDL searches at the 8 TeV LHC in section 3 in a simplified model framework with a single scalar or pseudoscalar heavy Higgs. We then turn to prospects for probing both scalar and pseudoscalar heavy Higgses in type II 2HDM at present and future colliders. We discuss the relevant backgrounds and introduce our analysis strategies in section 4. We present the results of these analyses in section 5 and we summarize our work in section 6. We reserve details of the BDT used in our 14 TeV and 100 TeV analyses for appendix A, and a discussion of the related bb associated production channel for appendix B.

2 The Higgs sector

For the sake of concreteness, in this work we will focus on extended Higgs sectors whose low-energy physics can be characterized by a two Higgs doublet model of type II, such as the Higgs sector of the MSSM. In addition to the SM-like Higgs boson, these sectors contain two heavy neutral Higgs bosons — one CP-even (H) and one CP-odd (A) — and a pair of charged Higgs bosons ($H^\pm$). The physics of these bosons is governed at tree level by a neutral mixing angle and the ratio of the Higgs vacuum expectation values $\tan\beta$. In the particular case of the MSSM, the neutral mixing angle is further fixed by the mass scale of the heavy Higgs bosons. Current Higgs coupling measurements require such extended Higgs sectors to be near an *alignment limit* of the parameter space [26–30], in which the couplings of the light CP-even Higgs scalar are Standard Model-like.

[1] Whenever we will mention in the following just one of these two conjugated processes, we implicitly mean both $pp \to \bar{t}HW^+b$ and $pp \to tHW^-\bar{b}$, together.

JHEP01(2017)018

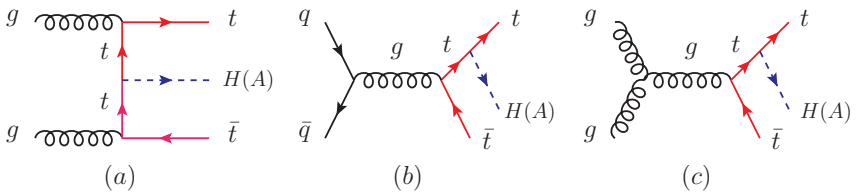

Figure 3. Typical Feynman diagrams for the production of a heavy scalar in association with a top pair at proton-proton colliders.

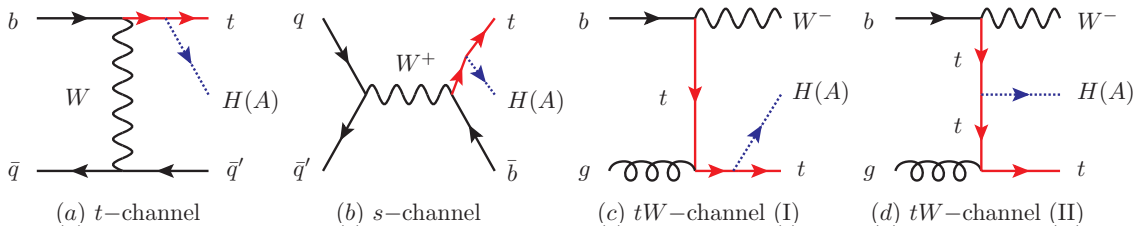

Figure 4. Typical Feynman diagrams for the production of a heavy scalar in association with a single top quark at proton-proton colliders.

2.1 Production of heavy scalars in association with top quark(s)

The physics of the alignment limit provides a natural organizing principle for associated production modes of the heavy Higgs bosons. In the alignment limit with small $\tan\beta$, the HW^+W^- and $b\bar{b}H(A)$ couplings are suppressed, so that the dominant contributions to $H(A)$ production arise from the $t\bar{t}H(A)$ vertex. This leads to a variety of production processes in association with $t\bar{t}$ pairs that can be generated from the standard model (SM) top production processes with an additional heavy scalar radiated from the internal top quark (figure 3a) or an external top quark leg (figure 3b and 3c).

In addition to production of a heavy Higgs in association with top quark pairs, production in association with a single top quark may play a useful role. Production of Higgs bosons in association with single top quarks was studied extensively in [31, 32], although the details differ somewhat near the alignment limit where radiation of heavy Higgses from vector bosons is suppressed. The production of a heavy scalar in association with a single top quark in the alignment limit contains three main channels: t-channel (figure 4a), s-channel (figure 4b) and tW-associated production channel (figure 4c and 4d). The s-channel process is highly suppressed by the center of mass energy $1/s^2$ and is much smaller than the other two. Although the t-channel process is suppressed by a factor of $\alpha/\left(\alpha_s \sin^2\theta_W\right)$, its cross-section is larger than that of the tW-associated channel on account of the larger phase space and the parton distribution function (PDF) of the valence quark. However, as shown in figure 4, the cross-section of the tW-associated channel for the heavy scalar with single top production is increased by the additional possibility of internal radiation. Furthermore, the suppression from the phase space volume is no longer significant when the scalar is heavy, because the volume of phase space is determined by the mass of the heavy scalar.

JHEP01(2017)018

Thus both the t-channel and tW-associated channels contribute significantly to the total cross section for production of a heavy Higgs boson in association with a single top quark.

Although a variety of search strategies are sensitive to this final state, in this work we focus on final states involving same-sign dileptons. If we require the signal events to contain SSDL, the contribution from the $tWH(A)$ channel will be enhanced by the possibility of the charged lepton from the $W^{\pm}$ decay. Hence we expect the dominant contributions from new physics in SSDL final states to come from the $tWH(A)$ channel, with a sub-dominant contribution coming from the $tqH(A)$ channel. The s-channel contribution should be negligibly small as discussed above.

In comparison, the rate for $t\bar{t}H(A)$ production is only slightly suppressed by the phase space, and is enhanced relative to single-top processes by both the coupling constant of the strong interaction $\mathcal{O}\left(\alpha_s \sin^2\theta_W/\alpha\right)$ and the gluon PDF. Hence the contributions from $t\bar{t}$ associated production are expected to be significant, especially when searching for SSDL signals. In this work we consider both single-top and $t\bar{t}$ associated production processes.

In what follows, we will both obtain existing limits on these processes by reinterpreting SSDL searches at $\sqrt{s} = 8\,\text{TeV}$ and forecast the reach of the $\sqrt{s} = 14\,\text{TeV}$ LHC and future pp-collider in SSDL channels. To do so, we work in terms of a simplified model in which $H(A)$ couples to the SM particles via

$$\mathcal{L} = -y_t(c_H H\bar{t}t + ic_A A\bar{t}\gamma_5 t)\,, \tag{2.1}$$

where y_t, y_b and y_τ are the SM Yukawa coupling constant of the third generation leptons. As we are focusing on the case with small $\tan\beta$ we will neglect the sub-dominant coupling to b and τ when we derive limits on the coefficients c_H, c_A.

We calculate the leading order (LO) cross-sections using `MadGraph` 5 [33] with CT14llo PDF in the 5-flavor scheme (FS) [34]. For the $tH(A) + X$ processes, we choose the factorization and renormalization scales to be $\mu_F = \mu_R = m_t^{\overline{\text{MS}}} + m_{H(A)}$, where $m_t^{\overline{\text{MS}}} = 163\,\text{GeV}$ is the $\overline{\text{MS}}$ mass of the SM top quark. For $t\bar{t}H(A)$ process, we instead choose $\mu_F = \mu_R = m_t^{\overline{\text{MS}}} + m_{H(A)}/2$. The resulting cross sections for the 8 TeV and 14 TeV LHC are shown in figure 5. Notice that the 4-top process has larger scale uncertainty since it is $\mathcal{O}\left(\alpha_s^2\right)$, while the 3-top processes are $\mathcal{O}\left(\alpha_s\right)$.

For the 14 TeV LHC and a future 100 TeV pp-collider we present additionally the contours in the m_A-$\tan\beta$ plane for the production cross-sections of the $pp \to t\bar{t}H(A)$ and the $pp \to tWH(A)$ processes within the framework of the MSSM in figure 6. We point out that for low masses the cross-section of the $tWH(A)$ processes is smaller than that of $t\bar{t}H(A)$ processes, but that the situation reverses at large heavy Higgs masses due to the asymptotic freedom of α_s together with the faster falloff in x of the gluon PDF relative to the bottom-quark PDF.

3 Constraint from LHC Run I

Before developing a strategy for future searches, it is useful to determine the state of existing limits from searches at the 8 TeV LHC. In this section, we find the constraint on

JHEP01(2017)018

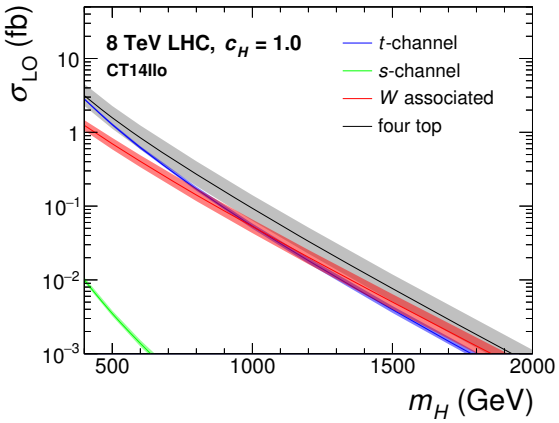

(a) CP-even heavy Higgs production at 8 TeV.

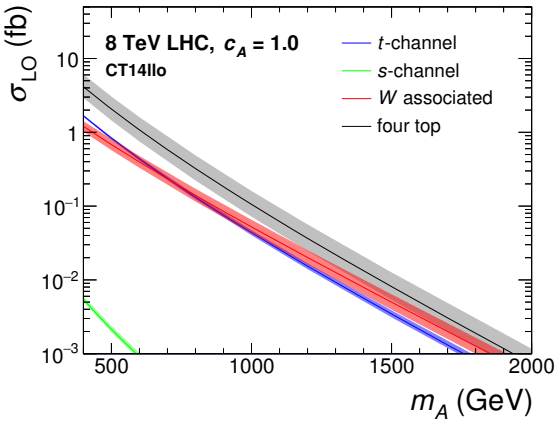

(b) CP-odd heavy Higgs production at 8 TeV.

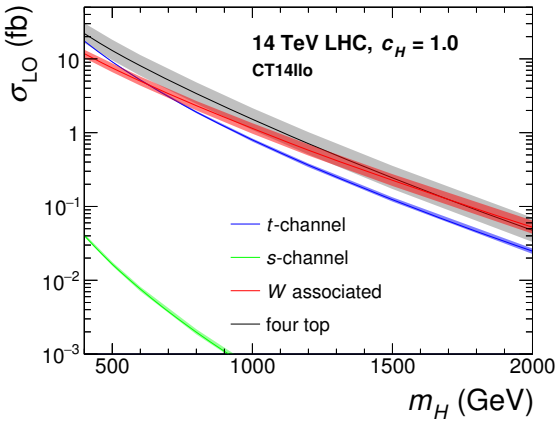

(c) CP-even heavy Higgs production at 14 TeV.

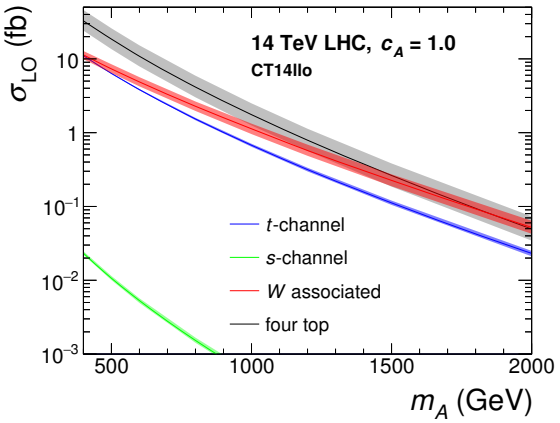

(d) CP-odd heavy Higgs production at 14 TeV.

Figure 5. (a) Cross-sections of the 3-top (colored) and 4-top (black) processes for a CP-even heavy Higgs at the 8 TeV LHC, where the number of top quarks includes both the associated states and the $t\bar{t}$ decay of the heavy Higgs. (b) The corresponding cross sections for a CP-odd heavy Higgs. (c) Cross-sections of the 3-top (colored) and 4-top (black) processes for a CP-even heavy Higgs at the 14 TeV. (d) The corresponding cross sections for a CP-odd heavy Higgs. In each case the shaded regions represent the scale uncertainties. Note the difference of uncertainties for processes proportional to α_s and α_s^2. In simulating these cross-sections we have assumed that the heavy Higgs coupling to bottom quarks and τ-lepton are negligible, which corresponds to small values of $\tan\beta$.

heavy Higgs bosons coming from an SSDL search performed by the CMS collaboration [35]. We consider a simplified model containing a heavy scalar or pseudoscalar Higgs boson with coupling to the top quark as in Equation (2.1). The three-top signal events are generated to leading order (LO) at parton level with CTEQ6L1 PDFs [36] within the 5-flavor scheme using `MadGraph` [33]. The renormalization and factorization scales are set to be $\mu_R = \mu_F = m_t + m_{H(A)}$. We also generate four-top signal events with the same method as the three-top signal events. The renormalization and factorization scales for four-top processes are set to be $\mu_R = \mu_F = m_t + m_{H(A)}/2$.

JHEP01(2017)018

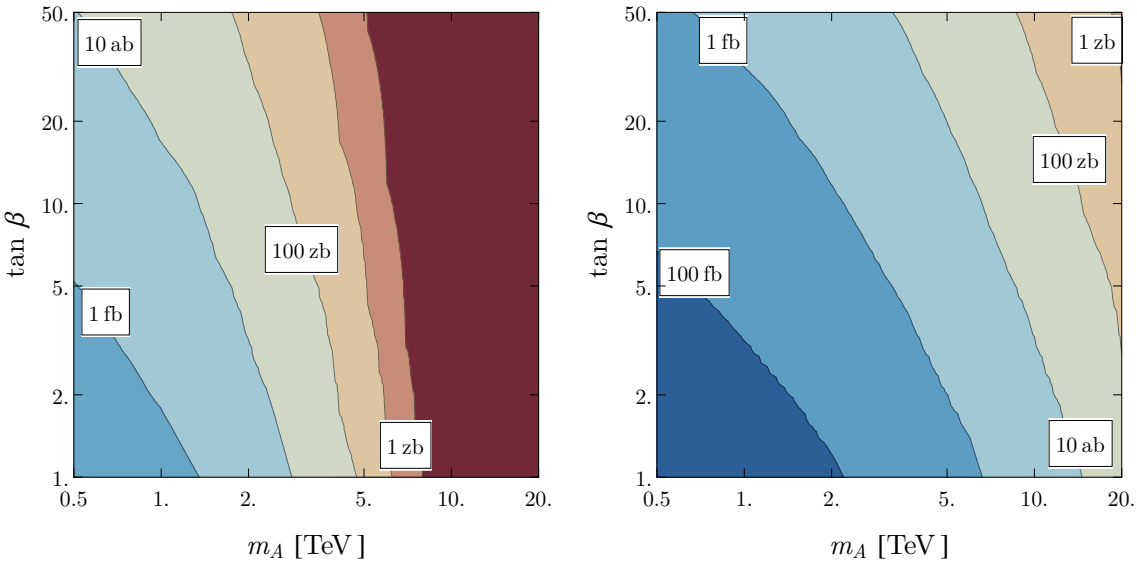

(a) $\sigma\,(pp \to (H+A)t\bar{t})$ at 14 TeV.

(b) $\sigma\,(pp \to (H+A)t\bar{t})$ at 100 TeV.

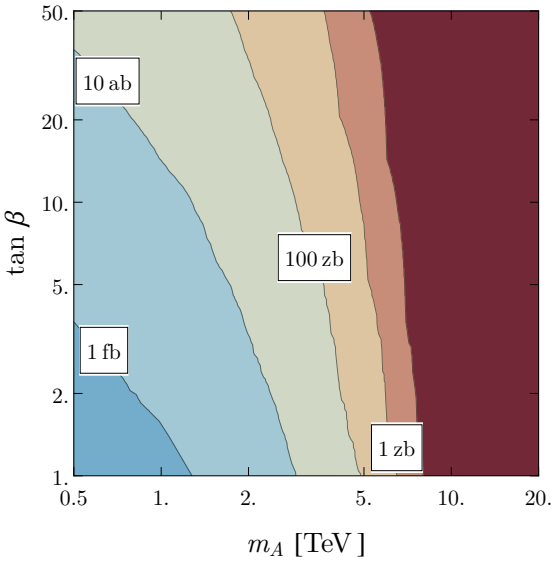

(c) $\sigma\,(pp \to (H+A)tW^{\pm})$ at 14 TeV.

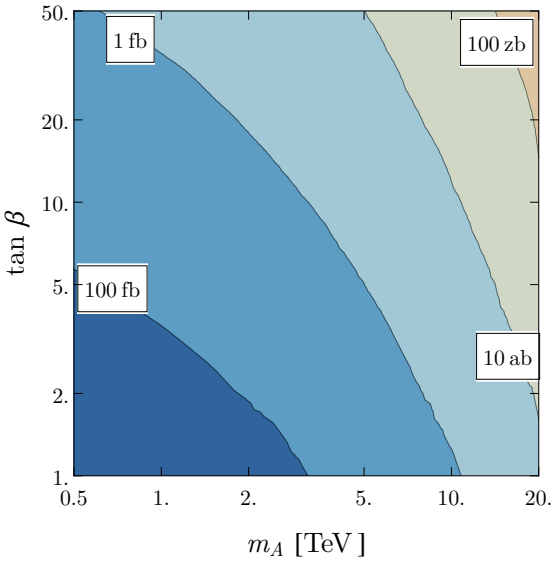

(d) $\sigma\,(pp \to (H+A)tW^{\pm})$ at 100 TeV.

Figure 6. (a) Contours of the $t\bar{t}(H+A)$ associated production cross-section of heavy neutral Higgs bosons at the 14 TeV LHC. (b) Contours of the $t\bar{t}(H+A)$ cross-sections at a 100 TeV pp-collider. (c) Contours of the $tW(H+A)$ associated production cross-section at the 14 TeV LHC. (d) Contours of the $tW(H+A)$ cross-sections at a 100 TeV pp-collider. The cross-section are calculated to leading order with `MadGraph` using its variable factorization and renormalization scale.

JHEP01(2017)018

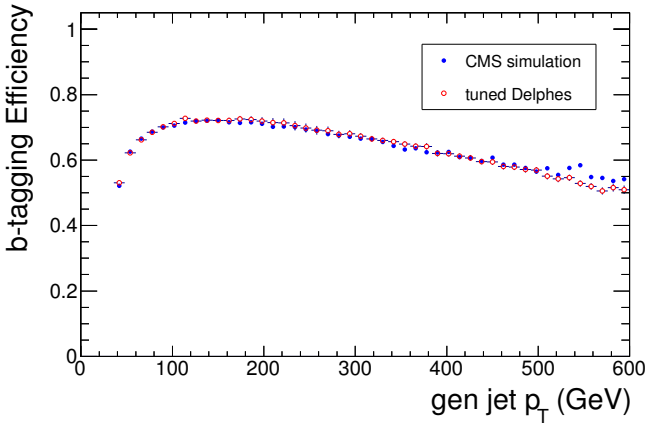

Figure 7. b-tagging efficiency as a function of jet p_T at the 8 TeV LHC. The red hollow points are the result from our simulation using $pp \to Zb(\bar{b})$ events. The solid blue points are the result from the CMS simulation presented in [35]. Although [35] uses simulated $t\bar{t}$ events, the b-tagging efficiency is not expected to differ substantially between different processes.

In both cases, the top quarks in the final state are decayed using `MadGraph` in order to preserve the effects of spin correlations. Events are showered using `PYTHIA` 6.4 [37] with the Z2 Tune [38]. `Delphes` 3 [39, 40] is used to simulate the detector effects. The b-tagging efficiency from `Delphes` is tuned to mimic the results of the simulation by the CMS collaboration (cf. figure 7). The mis-tagging rate of charm jets (light jets) is 20 % (1 %) [35]. We check the cut acceptances of events with same-sign top-quark pair production. The same-sign top search regions are defined as having ≥ 2 jets, $E_T^{\text{miss}} > 30\,\text{GeV}$ and $H_T > 80\,\text{GeV}$. Additionally, the number of b-jets has to be either equal to one (SStop1) or greater than one (SStop2). The SStop1 (SStop2) search region acceptance (including branching fractions) is 0.43 % (0.26 %) with relative uncertainty 14 % from simulation by the CMS collaboration [35], while our result is 0.39 % (0.28 %). The results of our simulation are consistent with the results given by the CMS collaboration to within the Monte Carlo uncertainty.

Given n observed events the significance is [41]

$$Z(x|n) = \sqrt{-2\ln\frac{L(x|n)}{L(n|n)}}\,, \tag{3.1}$$

where x is either the number of events predicted by the background only hypothesis b or by the background with signal hypothesis $b+s$ and the likelihood function is given by the Poisson probability

$$L(x|n) = \frac{x^n e^{-x}}{n!}\,. \tag{3.2}$$

For the exclusion of a model we require $Z(b+s|n) \geq 2$ and for discovery we require $Z(b|n) \geq 5$.[2] For the projection to future experiments we replace the event number n with the prediction for the alternative hypothesis. Hence, we are using $Z(b+s|b) \geq 2$ and $Z(b|b+$

[2]In the case that $n < b$ we calculate the significance with the more conservative statistics also used at the Tevatron, namely $Z = \sqrt{-2\ln\frac{L(b+s|n)}{L(b|n)}}$. This split approach corresponds to the test statistic $\tilde{q}_\mu$ in [41].

JHEP01(2017)018

$N_{b\text{-jets}}$	$p_T(l)$ [GeV]	E_T^{miss} [GeV]							
		50–120				> 120			
		H_T [GeV]				H_T [GeV]			
		200–400		> 400		200–400		> 400	
		N_{jets}		N_{jets}		N_{jets}		N_{jets}	
		2–3	≥ 4	2–3	≥ 4	2–3	≥ 4	2–3	≥ 4
0		SR01	SR03	SR02	SR04	SR05	SR07	SR06	SR08
	> 10	22	9.6	15	3.2	12	3.3	15	4.2
	> 20	13	4.0	10	2.8	4.4	2.8	10	4.4
1		SR11	SR13	SR12	SR14	SR15	SR17	SR16	SR18
	> 10	22	7.5	5.1	4.0	4.9	4.0	5.4	12
	> 20	7.5	4.0	7.1	2.8	8.0	5.1	3.2	9.7
≥ 2		SR21	SR23	SR22	SR24	SR25	SR27	SR26	SR28
	> 10	10	5.4	3.1	15	2.7	2.0	5.0	4.5
	> 20	13	4.3	3.5	11	6.5	2.0	3.7	4.1

Table 1. The $2\,\sigma$ upper bounds of the number of signal events for each signal region (SR) defined in [35].

$s) \geq 5$, for exclusion and discovery, respectively. Here we assume positive interference between signal and background and the systematic uncertainties of the signal and the background estimation are not included in this simplified statistical procedure. Using the result in table 7 of [35], we can give the $2\,\sigma$ upper bound of the event numbers of the new physics model for each signal region defined in [35]. The results are summarized in table 1.

Given a number of signal events s with $c_X = 1$ (where $X = H, A$) and an observed upper bound n in the same signal region, the central value of the upper bound on c_X is given by

$$c_X = \sqrt{\frac{n}{s}}\,. \tag{3.3}$$

The corresponding error on the bound on c_X is

$$\delta c_{\pm} = \frac{\delta n}{2\sqrt{ns}} = \frac{c_X}{2\sqrt{n}}\,. \tag{3.4}$$

We check all of the 24 signal regions (SR01–SR08, SR11–SR18, SR21–SR28) for H and A with $m_{H(A)} = 400, 500, 600, 800, 1000\,\text{GeV}$. The numerical simulation indicates that the strongest constraint is from the "Low-p_T SR28" signal region for all of the mass points. For each mass point we consider the contributions from the t-channel, s-channel, W associated production channel and 4-top channel separately and in combination. As shown in table 2, the strongest constraint is from the 4-top channel as expected. The combined results are shown in figure 8. From this it is apparent that 8 TeV results place no meaningful limit on heavy scalar or pseudoscalar Higgses decaying to $t\bar{t}$ with $c_H, c_A \lesssim 4$.

JHEP01(2017)018

Mass [GeV]		t-channel	s-channel	W associated	4-top
400	c_H	10.3 ± 2.43	91.7 ± 21.6	7.98 ± 1.87	4.47 ± 1.06
	c_A	9.63 ± 2.27	123 ± 29.0	8.40 ± 1.98	4.28 ± 1.01
500	c_H	9.26 ± 2.19	130 ± 30.7	9.55 ± 2.24	5.81 ± 1.37
	c_A	11.4 ± 2.69	163 ± 38.4	9.89 ± 2.33	5.37 ± 1.27
600	c_H	12.0 ± 2.83	186 ± 43.9	12.0 ± 2.82	7.55 ± 1.78
	c_A	19.9 ± 4.69	228 ± 53.5	12.3 ± 2.90	6.99 ± 1.65
800	c_H	20.5 ± 4.83	531 ± 125	19.5 ± 4.56	12.7 ± 3.00
	c_A	23.6 ± 5.55	441 ± 104	19.6 ± 4.62	11.9 ± 2.81
1000	c_H	36.2 ± 8.55	760 ± 179	32.1 ± 7.52	21.5 ± 5.05
	c_A	40.0 ± 9.45	848 ± 200	32.1 ± 7.55	20.2 ± 4.76

Table 2. The $2\,\sigma$ upper bounds of the effective interaction strength c_H and c_A from 8 TeV LHC.

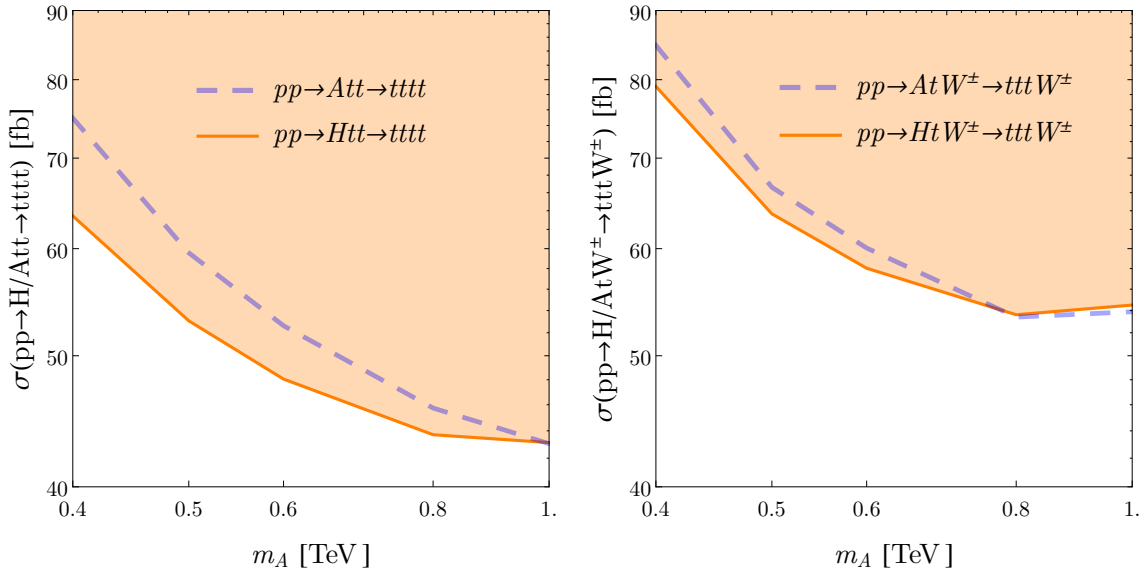

(a) 4-top. (b) 3-top.

Figure 8. (a) Exclusion cross section for $pp \to H/Att \to tttt$ using 8 TeV LHC data. (b) Exclusion cross section for $pp \to A/HtW^{\pm} \to tttW^{\pm}$ using 8 TeV LHC data.

4 Analysis strategies for future searches

We next consider the prospects for optimized searches at the 14 TeV LHC and a future 100 TeV pp collider. We consider both a cut-based analysis and a BDT analysis at 14 TeV, the former providing a validation of the latter. For our 100 TeV projections we consider only a BDT analysis for simplicity, given the considerable uncertainty regarding the parameters of a 100 TeV collider. For all of these analyses we generate events in the four FS using `MadGraph` 2.3.3, such that the $tW^{\pm}H(A)$ signal is generated with an additional soft and for-

JHEP01(2017)018

Background	14 TeV		100 TeV	
	σ [fb]	$\mathcal{L}_{\text{gen}}$ [ab^{-1}]	σ [fb]	$\mathcal{L}_{\text{gen}}$ [ab^{-1}]
$t\bar{t}t\bar{t}$	0.4851	103	122.7	1.63
$tttW^{\pm}b$	0.06016	831	14.86	6.73
$t\bar{t}W^{+}b\bar{b}$	0.03284	1520	0.3822	262

Table 3. Leading order cross-section times branching ratio to same-sign dileptons for the dominant backgrounds at 14 TeV and 100 TeV, defined such that $tttW^{\pm}b$ does not have an overlapping contribution with $t\bar{t}t\bar{t}$. We have checked that $t\bar{t}W^{-}b\bar{b}$ is sub-dominant to $t\bar{t}W^{+}b\bar{b}$ at pp colliders and will neglect it in the further discussion.

ward/backward b-quark. We consider only events with jets harder than 20 GeV for the LHC and 40 GeV a future collider, respectively. We have kept the spin correlation using `MadSpin`.

We generate the dominant irreducible backgrounds $t\bar{t}t\bar{t}$ and $tttW^{\pm}b$, as well as the main reducible background $t\bar{t}W^{+}bb$. Given that our main analysis strategy involves SSDL, a mass-window cut around the Z peak, at least four b-jets and a veto on the third lepton, we have verified that the background contributions from $t\bar{t}W^{\pm}Z$, $t\bar{t}W^{\pm}cc$, $t\bar{t}Z$, $t\bar{t}h$ and $ttW^{\pm}$ are sub-dominant to the main backgrounds. The generated processes, their cross-sections, and the generated luminosity are summarized in table 3.

We use `Delphes` 3 to simulate a detector with CMS geometry. For the 14 TeV LHC, we use a tracker coverage of $|\eta| < 2.5$. We assume a tracker coverage of $|\eta| < 3.5$ for detectors at future 100 TeV colliders. For all analyses we use anti-k_T jet clustering with a jet cone size of 0.5. However, in the BDT-based analysis this parameter plays a tangential role, as we additionally consider exclusively defined sub-jets as well as objects built of multiple jets.

4.1 Pre-selection cuts

For the analyses covering the 14 TeV LHC we apply the following pre-selection cuts: we consider only events with exactly two leptons with identical charge and transverse momenta $p_T > 15$ GeV. The leptons must be isolated with an isolation radius of $\Delta R > 0.3$ and a maximal transverse momentum ratio of 0.2. Where the transverse momentum ratio is defined between the lepton and other cell activity within the isolation cone. If the lepton transverse momentum is larger than 50 GeV, we do not require them to be isolated [42]. We veto on a third lepton with $p_T > 10$ GeV. Additionally we require a minimal missing transverse energy $E_T^{\text{miss}} > 30$ GeV and reject events with less than four jets.

For the 100 TeV analysis we demand for the leading lepton a transverse momentum of 100 GeV. The second leading lepton must have a $p_T > 50$ GeV and we veto on a third lepton with $p_T > 50$ GeV. We do not require leptons to be isolated as long as they are harder than 100 GeV. Otherwise, we apply the same isolation cone parameter as in the case of the LHC. The missing transverse energy must be $E_T^{\text{miss}} > 60$ GeV.

JHEP01(2017)018

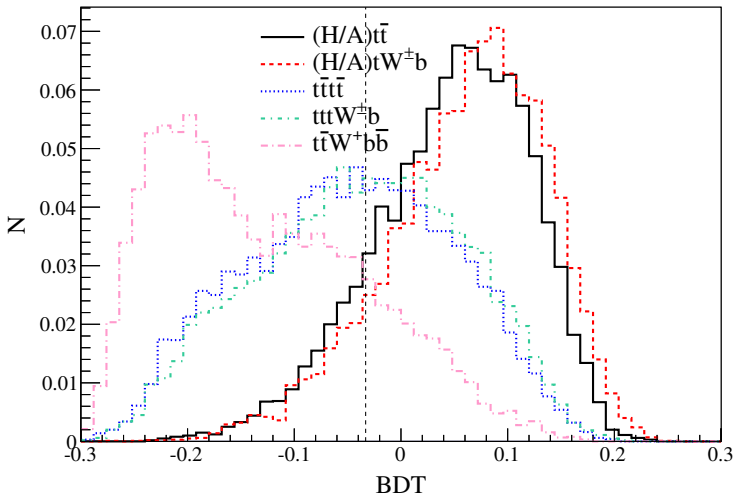

Figure 9. Example of a BDT result for the 14 TeV LHC and a Higgs mass of 1 TeV. While the Higgs produced in association with two (black) and one (red) top quark has large BDT values, the intrinsic background $t\bar{t}t\bar{t}$ (blue), $tttW^{\pm}b$ (green) and $ttW^{+}bb$ (pink) has small BDT values. The vertical line indicates the optimal cut, which maximizes the significance.

4.2 Cut-based analysis for 14 TeV

For the cut based analysis we use the `BoCA` b-tag presented in appendix A and require a minimum b-jet p_T of 40 GeV. For this analysis we follow the ideas in [43]. We require at least four bottom jets and veto events if the invariant mass of an electron pair falls within a 20 GeV window around the Z-peak. We develop a cut strategy by using the rectangular cut optimization of the `TMVA` library [44]. The dominant cut is on the scalar sum of transverse momenta H_T. In order to probe a given Higgs mass $m_{H/A}$ we require $H_T > m_{H/A}$. These cuts also ensure the suppression of instrumental backgrounds, especially the misidentification of jets as well as the misidentification of lepton charges [45].

4.3 BDT analysis for 14 and 100 TeV

We focus the BDT-based search strategy on the the main features of this signal, namely

- Same sign di-lepton (SSDL)
- Heavy Higgs boson resonance
- Two additional forward/backward b-quarks

We apply a series of BDT-taggers designed to reconstruct the complete signal signature from its decay components following the strategy presented in [15]. Our code is based on `FastJet` 3.1.3 [40] and the `TMVA` 4.2.1 library [44] of the `ROOT` framework [46] and is published as `BoCA` 0.2 [47]. We tag bottom-like jets, based on their displaced vertices. We exploit the fact that boosted top-like jets also show displacement but have additionally a larger jet mass. Furthermore we require or veto hard leptons inside the jet radius for

JHEP01(2017)018

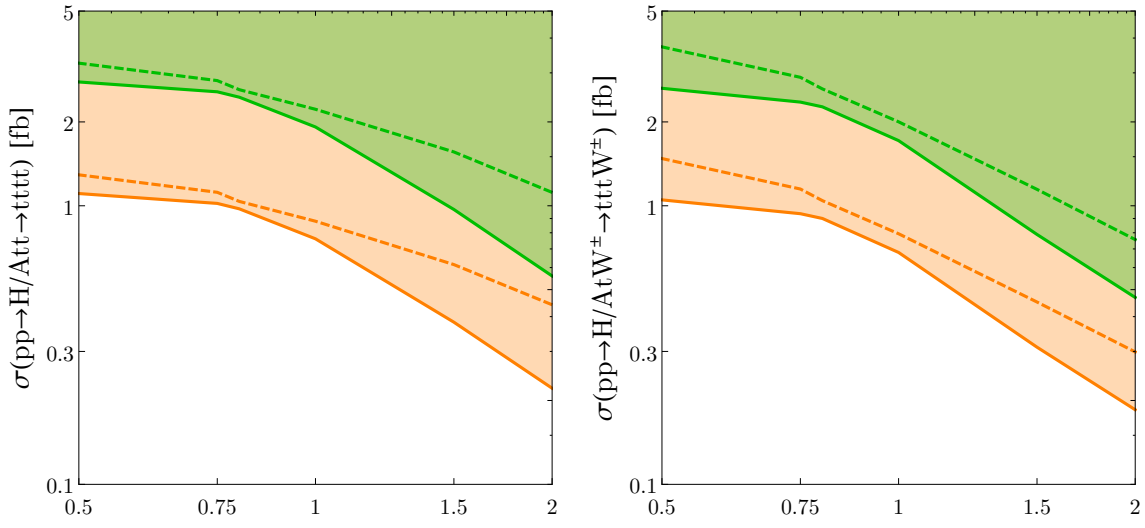

(a) $pp \to t\bar{t}H(A) \to t\bar{t}t\bar{t}$. (b) $pp \to tWH(A) \to tW^{\pm}t\bar{t}$.

Figure 10. (a) Model independent exclusion (orange) and discovery (green) limits at the 14 TeV LHC in the four-top channel. (b) Exclusion (orange) and discovery (green) limits in the three-top channel. The dashed limits are derived with the cut based analysis presented in section 4.2 while the solid limits are derived with the BDT analysis presented in section 4.3.

hadronic and leptonic top jets, respectively. In the case of un-boosted top quarks we reconstruct the tops from their spatially separated decay products. For the reconstruction of the heavy Higgs bosons we require two tagged top-like objects. We do not reconstruct the tops of the quark pair accompanying the heavy Higgs. Instead we require two jets with large $\Delta\eta$ and high b-likeliness. Finally we assume that one of the tops originating from the heavy Higgs decay, decays leptonically; that another lepton is present; and that these leptons have the same charge. One example of the final BDT result at 14 TeV is presented in figure 9.

5 Results

Here we present the results of the cut-based and BDT analyses presented in the previous section. We note that in section 3 we presented limits individually for scalar and pseudoscalar Higgs bosons in the context of a simplified model, as 8 TeV data is insufficient to meaningfully constrain the parameter space of the MSSM. In what follows, we present limits for the sum of scalar and pseudoscalar Higgs bosons in the parameter space of m_A and $\tan\beta$. We do so with an eye towards forecasting sensitivity to MSSM-like type II 2HDM in which the heavy scalar and pseudoscalar Higgs bosons are nearly degenerate.

5.1 Cut-based and BDT analyses at the 14 TeV LHC

The model-independent results for cut- and BDT-based analyses at the 14 TeV LHC are depicted separately for the three- and four-top channels in figure 10. While the cut-based

JHEP01(2017)018

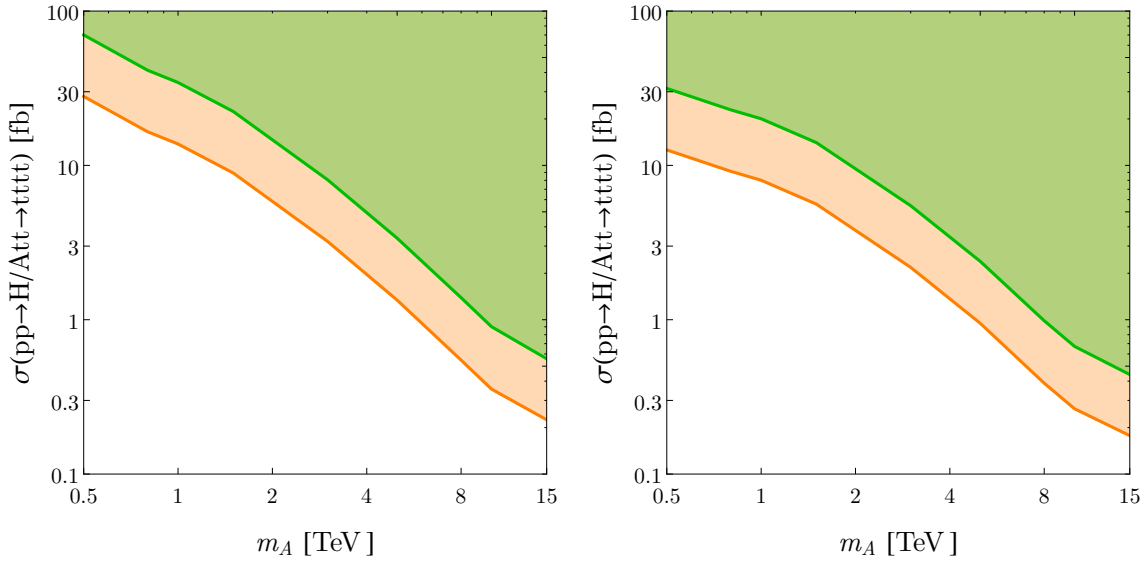

(a) $pp \to t\bar{t}H(A) \to t\bar{t}t\bar{t}$.

(b) $pp \to tW^{\pm}H(A) \to tW^{\pm}t\bar{t}$.

Figure 11. (a) Model independent limits for a future 100 TeV collider in the $t\bar{t}t\bar{t}$ channel. (b) Limits for a future 100 TeV collider in the $t\bar{t}tW^{\pm}$ channel. Note the dominance of the three-top channel over the four-top channel especially for low masses, due to the harder lepton originating from the $W^{\pm}$ decay compared to the top decay (cf. figure 2).

and BDT analyses have comparable sensitivity for lower masses, for larger masses the BDT-based strategy demonstrates its power as the reconstructed heavy Higgs resonance improves discrimination of signal from background. Furthermore, we would like to point out that the BDT-based analysis has an advantage in suppressing the signal over background ratio, as discussed in appendix B. We present the combined model dependent results of the BDT analysis in figure 12; the shaded purple regions denote the reach of the 14 TeV LHC with 300 and 3000 fb^{-1}. As shown in figure 12a the top associated heavy Higgs production can exclude the lower $\tan\beta$ region up to 1 and 1.8 TeV for 300 and 3000 fb^{-1}, respectively. The discovery reach of the LHC presented in figure 12b extends to 700 and 1100 GeV for the same luminosities. As already demonstrated in [15] the bottom associated heavy Higgs production covers the intermediate $\tan\beta$ region up to 1 TeV with 3000 fb^{-1}.[3]

5.2 BDT analysis at a 100 TeV *pp*-collider

The model-independent sensitivity of a 100 TeV collider is presented separately for the three- and four-top channels in figure 11. The model-dependent combination of three- and four-top channels is depicted alongside the 14 TeV LHC reach in figure 12. The top associated heavy Higgs production can exclude the lower $\tan\beta$ range up to 15 and 18 TeV for 3 and 30 ab^{-1}, respectively. The discovery reach extends to 10 and 15 TeV for the same luminosities. Of course, large uncertainties regarding detector properties, backgrounds,

[3]The slight change in the shape of the limits derived from the bottom associated Higgs production with decays to a top pair compared to [15] is the result of a combination of improved background simulation and correspondingly optimized analysis.

JHEP01(2017)018

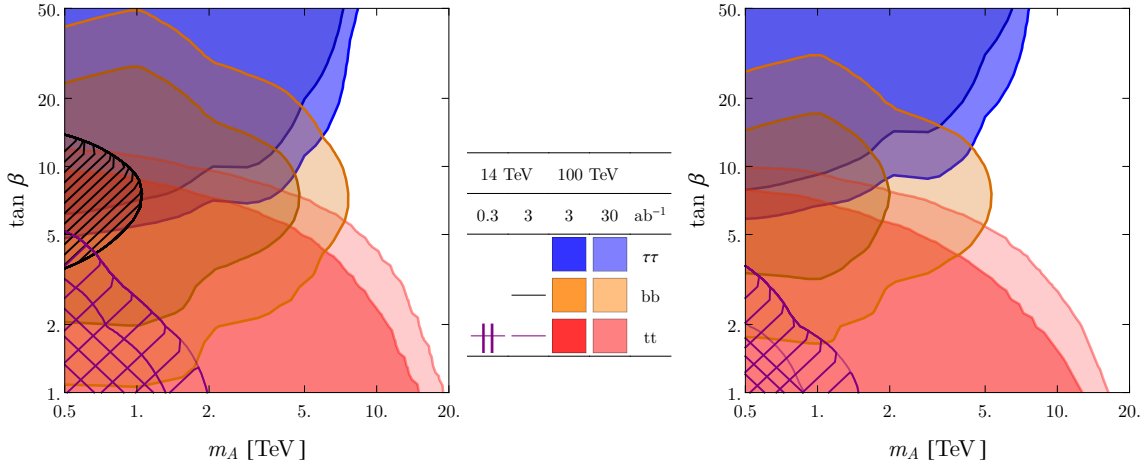

(a) Exclusion limits.

(b) Discovery limits.

Figure 12. Model dependent exclusion (a) and discovery (b) limits for the 14 TeV LHC (hatched in black and purple) and a 100 TeV hadron collider (colored) derived with the BDT analysis presented in section 4.3. The smaller bound can be reached with 0.3 and 3 ab^{-1} while the large bound can be reached with 3 and 30 ab^{-1} at the LHC and a future pp-collider, respectively. The low $\tan\beta$ region (red) is covered by the top associated heavy Higgs production with decays to top pairs. While the contribution from the $H/Ab\bar{b}$ vertex dominates the decays for large $\tan\beta$ we neglected its sub-leading contribution in the analysis covering small $\tan\beta$. The intermediate $\tan\beta$ region (orange) is covered by the bottom associated heavy Higgs production with decays to a top pair. The large $\tan\beta$ region (blue) is covered by the bottom associated heavy Higgs production with decays to τ lepton pairs. The latter two analyses are discussed in [15], and we revisit some aspects of the analysis in appendix B.

and BDT performance at 100 TeV make these limits approximate. The complementary bottom associated heavy Higgs production mode can be used to exclude the intermediate $\tan\beta$ region up to 4 and 8 GeV for 3 and 30 ab^{-1}, respectively. Finally the associated heavy Higgs production with two bottom quarks and decays to a τ lepton pair covers the large $\tan\beta$ range. Together, these channels cover the whole $\tan\beta$ range up to ~ 10 TeV.

Combining the dominance of the three-top channel over the four-top channel in figure 11 with the larger cross-section of the three-top channel compared to the four-top channel observed in figure 6, the $H(A)W^{\pm}b$ channel provides the main contribution to the limits presented in figure 12.

6 Summary and outlook

Heavy Higgs bosons decaying predominantly into $t\bar{t}$ final states pose an exceptional challenge to searches at hadron colliders, particularly when $b\bar{b}$ associated production is negligible. This makes it difficult to probe a variety of motivated theories with heavy Higgs bosons decaying to $t\bar{t}$, including most notably the low $\tan\beta$ region of the MSSM Higgs sector. In this work we have proposed probing this parameter space by searching for heavy Higgses produced in association with one and two top quarks. While these processes may

JHEP01(2017)018

be probed in a variety of final states, we have focused on searches involving same-sign dilepton pairs. We have shown that existing LHC searches at 8 TeV are sensitive to these channels, though current limits are too weak to meaningfully constrain the parameter space of heavy Higgs bosons. However, the refinement of these cut-based searches at 14 TeV will begin to meaningfully constrain the relevant parameter space. Further improvement with BDT-based analyses can potentially cover the lower part of the m_A-$\tan\beta$ plain up to 700–1800 GeV and 10–18 TeV at the LHC and a future hadron collider, respectively. Together with the results of [14, 15] we have shown that the complete $\tan\beta$ range can be covered with associated heavy Higgs production, while only the upper part of this range can be probed up to large masses with resonantly-produced heavy Higgs bosons. Although the sensitivity reach was displayed in type II 2HDM in this article, the proposed strategies can be applied to probe low $\tan\beta$ region of the 2HDM of the other types as well. The sensitivity projection is straightforward.

Acknowledgments

J. Hajer is supported by the Collaborative Research Fund (CRF) HUKST4/CRF/13G. Y.-Y. Li is supported by the Hong Kong PhD Fellowship Scheme (HKPFS). T. Liu is supported by the General Research Fund (GRF) under Grant No. 16304315 and 16312716. Both the HKPFS and the CRF, GRF grants are issued by the Research Grants Council of Hong Kong S.A.R.. N. Craig is supported by the U.S. DOE under contract No. DE-SC0014129. H. Zhang is supported by the U.S. DOE under contract No. DE-SC0011702.

A Acceptances of the BoCA SM taggers

In order to test the BoCA SM taggers, we have generated event files containing particle pairs generated via t- and s-channel contributions. During the analysis we have required exactly one particle and one jet to fall inside the required transverse momentum window.

The BoCA bottom tagger exploits the longevity of B-mesons produced in the bottom decay and uses the radial displacement of jet tracks in order to discriminate against other jets. The track positions provided by Delphes are smeared and serve as a starting point for the calculation of displacement observables, such as the track multiplicity, average displacement of tracks and the invariant mass of the displaced tracks. We do not attempt to reconstruct secondary jet vertices. The signal and background acceptances for jets with $500\,\text{GeV} < p_T < 600\,\text{GeV}$ as well as a representation of the BDT response are presented in figure 13. Using a BDT-cut of 0.05 leads to a b-tagging rate of 71 % with a c-jet fake rate of 18 %, while the misidentification rate for light quarks and gluon jets is 1.4 % and 6.4 %, respectively.

The BoCA tagger for hadronically decaying tops is based on the bottom tagger and a W-tagger. Additionally, it takes the kinematic variables between these two particles into account, such as the rapidity difference and the opening angle ΔR. Two representations of the top tagger BDT response are shown in figure 14. In order to compare the performance of the BoCA top tagger to existing top taggers, we have incorporated the HEPTopTagger [48]

JHEP01(2017)018

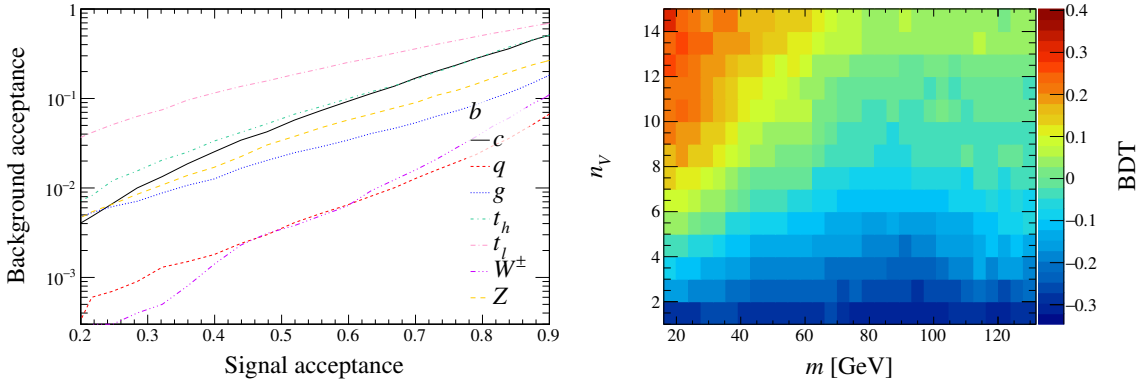

(a) Acceptances. (b) BDT over mass and multiplicity.

Figure 13. BoCA bottom tagger. (a) Acceptances for jets with a transverse momentum of 500 GeV $< p_T <$ 600 GeV at the 14 TeV LHC. (b) Distribution of averaged BDT values after projection of the parameter space onto the plane spanned by the jet mass (m) and the track multiplicity (n_V). Low BDT values (blue) are background-like and high BDT values (red) are signal-like. We require the final state particles to have transverse momenta larger than 500 GeV to make sure that the induced two jets are well-separated.

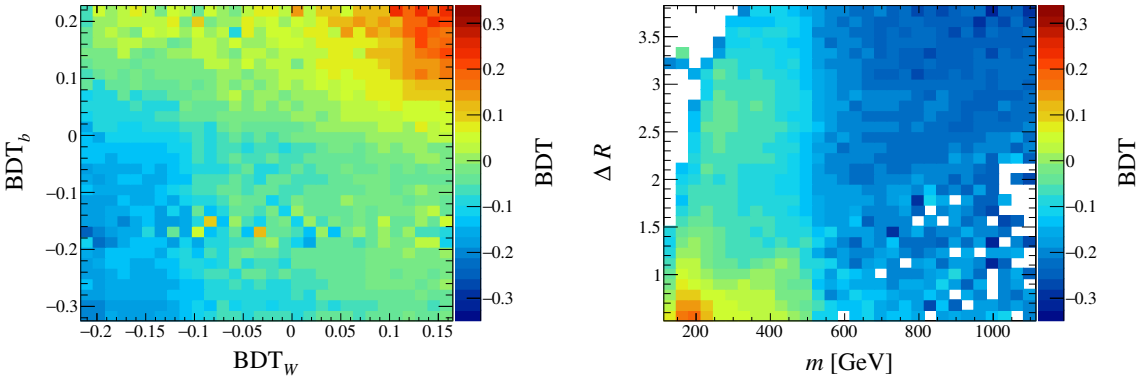

(a) W and b BDT. (b) Top mass and opening angle.

Figure 14. Examples of the top tagger BDT response. (a) Averaged BDT response after projection of the parameter space onto the plane spanned by the W BDT and the b BDT. (b) Averaged BDT response after projection onto the plane spanned by the top mass (m) and the opening angle (ΔR). Low BDT values (blue) are background-like and high BDT values (red) are signal-like.

into the BoCA code.[4] While the HEPTopTagger is optimized for top (fat-)jet tagging the BoCA top-tagger also combines multiple jets in order to reconstruct less boosted top jets. For the purposes of comparison, we require exactly one top particle and one reconstructed top to have a transverse momentum between 750 GeV $< p_T <$ 1 TeV. In order to create a range of signal acceptances with the HEPTopTagger we initially do not cut on the top mass but use the freedom in this parameter to tune the signal acceptance. The receiver

[4]During finalization of this article the code for the second version of the HEPTopTagger [49] has been published. We leave the comparison of the BoCA top tagger to this new version for a future publication.

JHEP01(2017)018

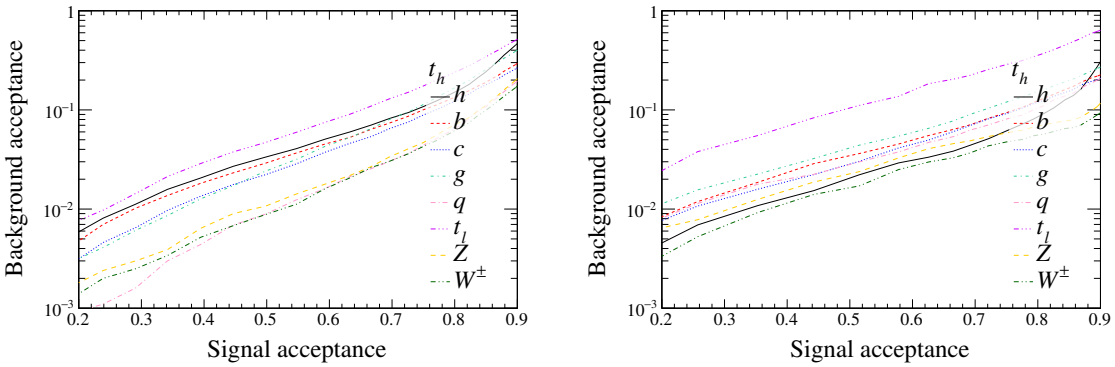

(a) `BoCA` top tagger. (b) `HEPTopTagger`.

Figure 15. Top tagger acceptances for top jets with an transverse momentum between 750 GeV $< p_T <$ 1 TeV at the 14 TeV LHC. (a) Signal acceptance calculated using the `BoCA` top tagger with `Delphes` jets with a jet cone size of 0.5. (b) Signal acceptance calculated using the `HEPTopTagger` without a prior on the top mass using optimally clustered jets with a jet cone size of 0.462.

operating characteristic (ROC) curves for the `BoCA` top tagger and the `HEPTopTagger` are presented in figure 15. The direct comparison in this energy range shows that the `BoCA` top tagger suppresses b and c jets as well as the `HEPTopTagger`, while it performs slightly better for gluon and W-boson jets. For light quarks, Z- and Higgs-boson jets it performs roughly twice as well as the `HEPTopTagger`.

B Comparison between cut- and BDT-based approaches in $pp \to Hbb$

In [15] we have analyzed the process $pp \to Hbb$ against the inclusive $t\bar{t}$ background. The authors of the recent publication [17] have attempted to exclude the same signal using a simple cut-based approach. Their conclusion is that the small signal over background ratio makes it impossible to exclude relevant models even when $\frac{s}{\sqrt{b}}$ is appreciable.[5] Hence we would like to explicitly demonstrate that a BDT-based approach improves the background rejection ($\frac{s}{b}$) to the level demanded in [17]. In order to ensure comparability we use figure 7 of [17] as a starting point for our discussion. The cross section of the model used in [17] as well as the best exclusion limit derived in this paper are plotted as dotted lines in figure 16. The cut-based analysis in [17] makes use of the transverse momenta of the four leading jets and the leading lepton, the scalar H_T, and the bottom number. We call this set of variables Var_1 and have applied it in both a cut- and a BDT-based analysis. Which leads to results comparable to those derived in [17]. In [15] we have reconstructed the complete event signature and used a large set of variables. This set of variables contains the BDT of all reconstructed objects, the ratios between their kinematic observables, as well as the pull [50] between these objects. Here we have only reconstructed the heavy Higgs boson and have applied Var_1 to

[5] The authors of [17] point out that they found a b-quark distribution which differs from the one presented in [15]. We have traced this difference back to deviations in the plot parameters. While we plot the b-quarks sorted by rapidity, the authors of [17] plot the b-quarks sorted by their transverse momentum. We thank the authors of [17] for clarifying their analysis.

JHEP01(2017)018

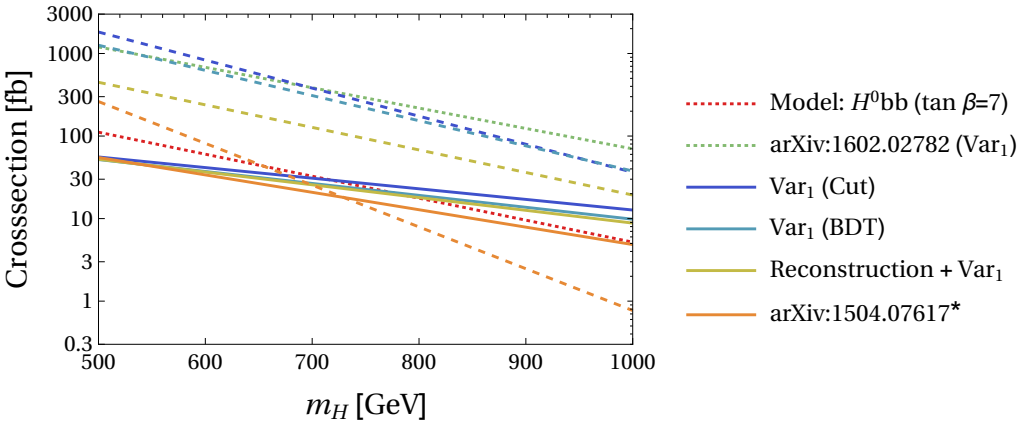

Figure 16. Comparison of model independent exclusion cross section requiring a significance of $Z(b+s|b) \geq 2$ (solid) and a background suppression of $\frac{s}{b} \geq 1\,\%$ (dashed). Applying the set of seven basic variables (Var$_1$ = $\{p_T(j_1)$, $p_T(j_2)$, $p_T(j_3)$, $p_T(j_4)$, $p_T(l_1)$, H_T, $\#b\}$) used in Reference [17] (dotted green) leads in our analysis to comparable results with both cut- and BDT based approaches (dashed blue). If we reconstruct the heavy Higgs boson and apply Var$_1$ (brown) we are able to significantly increase the background suppression. Using the technique described in [15] with the lepton isolation used in this publication (orange) leads once more to a notable improvement. In [15] we have only considered hard leptons, in this analysis we use hard leptons as well as isolated soft leptons. In the legend we use "*" to denote this difference.

suppress the background. For low masses this improves the significance marginally, but the ratio between signal and background is increased significantly. Finally, using the complete technique of [15] leads to a background suppression of $\mathcal{O}\,(0.2\text{–}6\,\%)$ on the boundary of the exclusion region for the HL-LHC. For a future 100 TeV collider the background suppression on the boundary of the exclusion region varies in the range 1–8 TeV between $\mathcal{O}\,(0.2\text{–}15\,\%)$.

References

[1] ATLAS collaboration, *Search for the neutral Higgs bosons of the minimal supersymmetric Standard Model in pp collisions at $\sqrt{s} = 7$ TeV with the ATLAS detector*, *JHEP* **02** (2013) 095 [arXiv:1211.6956] [INSPIRE].

[2] ATLAS collaboration, *Search for neutral Higgs bosons of the minimal supersymmetric Standard Model in pp collisions at $\sqrt{s} = 8$ TeV with the ATLAS detector*, *JHEP* **11** (2014) 056 [arXiv:1409.6064] [INSPIRE].

[3] ATLAS collaboration, *Search for a CP-odd Higgs boson decaying to Zh in pp collisions at $\sqrt{s} = 8$ TeV with the ATLAS detector*, *Phys. Lett.* **B 744** (2015) 163 [arXiv:1502.04478] [INSPIRE].

JHEP01(2017)018

[4] ATLAS collaboration, *Search for an additional, heavy Higgs boson in the $H \to ZZ$ decay channel at $\sqrt{s} = 8$ TeV in pp collision data with the ATLAS detector*, *Eur. Phys. J.* **C 76** (2016) 45 [arXiv:1507.05930] [INSPIRE].

[5] ATLAS collaboration, *Constraints on non-Standard Model Higgs boson interactions in an effective Lagrangian using differential cross sections measured in the $H \to \gamma\gamma$ decay channel at $\sqrt{s} = 8$ TeV with the ATLAS detector*, *Phys. Lett.* **B 753** (2016) 69 [arXiv:1508.02507] [INSPIRE].

[6] ATLAS collaboration, *Search for a high-mass Higgs boson decaying to a W boson pair in pp collisions at $\sqrt{s} = 8$ TeV with the ATLAS detector*, *JHEP* **01** (2016) 032 [arXiv:1509.00389] [INSPIRE].

[7] CMS collaboration, *Searches for heavy Higgs bosons in two-Higgs-doublet models and for $t \to ch$ decay using multilepton and diphoton final states in pp collisions at 8 TeV*, *Phys. Rev.* **D 90** (2014) 112013 [arXiv:1410.2751] [INSPIRE].

[8] CMS collaboration, *Search for neutral MSSM Higgs bosons decaying into a pair of bottom quarks*, *JHEP* **11** (2015) 071 [arXiv:1506.08329] [INSPIRE].

[9] CMS collaboration, *Search for neutral MSSM Higgs bosons decaying to $\mu^+\mu^-$ in pp collisions at $\sqrt{s} = 7$ and 8 TeV*, *Phys. Lett.* **B 752** (2016) 221 [arXiv:1508.01437] [INSPIRE].

[10] ATLAS collaboration, *Search for charged Higgs bosons decaying via $H^\pm \to \tau^\pm\nu$ in fully hadronic final states using pp collision data at $\sqrt{s} = 8$ TeV with the ATLAS detector*, *JHEP* **03** (2015) 088 [arXiv:1412.6663] [INSPIRE].

[11] ATLAS collaboration, *Search for a charged Higgs boson produced in the vector-boson fusion mode with decay $H^\pm \to W^\pm Z$ using pp collisions at $\sqrt{s} = 8$ TeV with the ATLAS experiment*, *Phys. Rev. Lett.* **114** (2015) 231801 [arXiv:1503.04233] [INSPIRE].

[12] CMS collaboration, *Search for a charged Higgs boson in pp collisions at $\sqrt{s} = 8$ TeV*, *JHEP* **11** (2015) 018 [arXiv:1508.07774] [INSPIRE].

[13] P.S. Bhupal Dev and A. Pilaftsis, *Maximally symmetric two Higgs doublet model with natural Standard Model alignment*, *JHEP* **12** (2014) 024 [*Erratum ibid.* **11** (2015) 147] [arXiv:1408.3405] [INSPIRE].

[14] N. Craig, F. D'Eramo, P. Draper, S. Thomas and H. Zhang, *The hunt for the rest of the Higgs bosons*, *JHEP* **06** (2015) 137 [arXiv:1504.04630] [INSPIRE].

[15] J. Hajer, Y.-Y. Li, T. Liu and J.F.H. Shiu, *Heavy Higgs bosons at 14 TeV and 100 TeV*, *JHEP* **11** (2015) 124 [arXiv:1504.07617] [INSPIRE].

[16] B. Bhattacherjee, A. Chakraborty and A. Choudhury, *Status of the MSSM Higgs sector using global analysis and direct search bounds and future prospects at the High Luminosity LHC*, *Phys. Rev.* **D 92** (2015) 093007 [arXiv:1504.04308] [INSPIRE].

[17] S. Gori, I.-W. Kim, N.R. Shah and K.M. Zurek, *Closing the wedge: search strategies for extended Higgs sectors with heavy flavor final states*, *Phys. Rev.* **D 93** (2016) 075038 [arXiv:1602.02782] [INSPIRE].

[18] K.J.F. Gaemers and F. Hoogeveen, *Higgs production and decay into heavy flavors with the gluon fusion mechanism*, *Phys. Lett.* **B 146** (1984) 347 [INSPIRE].

[19] D. Dicus, A. Stange and S. Willenbrock, *Higgs decay to top quarks at hadron colliders*, *Phys. Lett.* **B 333** (1994) 126 [hep-ph/9404359] [INSPIRE].

JHEP01(2017)018

[20] R. Frederix and F. Maltoni, *Top pair invariant mass distribution: a window on new physics*, *JHEP* **01** (2009) 047 [arXiv:0712.2355] [INSPIRE].

[21] S. Jung, J. Song and Y.W. Yoon, *Dip or nothingness of a Higgs resonance from the interference with a complex phase*, *Phys. Rev.* **D 92** (2015) 055009 [arXiv:1505.00291] [INSPIRE].

[22] T. Han, G. Valencia and Y. Wang, *Hadron collider signatures for new interactions of top and bottom quarks*, *Phys. Rev.* **D 70** (2004) 034002 [hep-ph/0405055] [INSPIRE].

[23] B. Lillie, J. Shu and T.M.P. Tait, *Top compositeness at the Tevatron and LHC*, *JHEP* **04** (2008) 087 [arXiv:0712.3057] [INSPIRE].

[24] B.S. Acharya, P. Grajek, G.L. Kane, E. Kuflik, K. Suruliz and L.-T. Wang, *Identifying multi-top events from gluino decay at the LHC*, arXiv:0901.3367 [INSPIRE].

[25] N. Chen, J. Li and Y. Liu, *LHC searches for heavy neutral Higgs bosons with a top jet substructure analysis*, *Phys. Rev.* **D 93** (2016) 095013 [arXiv:1509.03848] [INSPIRE].

[26] J.F. Gunion and H.E. Haber, *The CP conserving two Higgs doublet model: the approach to the decoupling limit*, *Phys. Rev.* **D 67** (2003) 075019 [hep-ph/0207010] [INSPIRE].

[27] N. Craig and S. Thomas, *Exclusive signals of an extended Higgs sector*, *JHEP* **11** (2012) 083 [arXiv:1207.4835] [INSPIRE].

[28] N. Craig, J. Galloway and S. Thomas, *Searching for signs of the second Higgs doublet*, arXiv:1305.2424 [INSPIRE].

[29] M. Carena, I. Low, N.R. Shah and C.E.M. Wagner, *Impersonating the Standard Model Higgs boson: alignment without decoupling*, *JHEP* **04** (2014) 015 [arXiv:1310.2248] [INSPIRE].

[30] H.E. Haber, *The Higgs data and the decoupling limit*, in 1st *Toyama International Workshop on Higgs as a Probe of New Physics* 2013 *(HPNP*2013*)*, Toyama Japan February 13–16 2013 [arXiv:1401.0152] [INSPIRE].

[31] F. Maltoni, K. Paul, T. Stelzer and S. Willenbrock, *Associated production of Higgs and single top at hadron colliders*, *Phys. Rev.* **D 64** (2001) 094023 [hep-ph/0106293] [INSPIRE].

[32] F. Demartin, F. Maltoni, K. Mawatari and M. Zaro, *Higgs production in association with a single top quark at the LHC*, *Eur. Phys. J.* **C 75** (2015) 267 [arXiv:1504.00611] [INSPIRE].

[33] J. Alwall et al., *The automated computation of tree-level and next-to-leading order differential cross sections and their matching to parton shower simulations*, *JHEP* **07** (2014) 079 [arXiv:1405.0301] [INSPIRE].

[34] S. Dulat et al., *New parton distribution functions from a global analysis of quantum chromodynamics*, *Phys. Rev.* **D 93** (2016) 033006 [arXiv:1506.07443] [INSPIRE].

[35] CMS collaboration, *Search for new physics in events with same-sign dileptons and jets in pp collisions at* $\sqrt{s} = 8$ *TeV*, *JHEP* **01** (2014) 163 [*Erratum ibid.* **01** (2015) 014] [arXiv:1311.6736] [INSPIRE].

[36] J. Pumplin, D.R. Stump, J. Huston, H.L. Lai, P.M. Nadolsky and W.K. Tung, *New generation of parton distributions with uncertainties from global QCD analysis*, *JHEP* **07** (2002) 012 [hep-ph/0201195] [INSPIRE].

[37] T. Sjöstrand, S. Mrenna and P.Z. Skands, *PYTHIA* 6.4 *physics and manual*, *JHEP* **05** (2006) 026 [hep-ph/0603175] [INSPIRE].

JHEP01(2017)018

[38] R. Field, *Min-bias and the underlying event at the LHC*, *Acta Phys. Polon.* **B 42** (2011) 2631 [arXiv:1110.5530] [INSPIRE].

[39] DELPHES 3 collaboration, J. de Favereau et al., *DELPHES 3, a modular framework for fast simulation of a generic collider experiment*, *JHEP* **02** (2014) 057 [arXiv:1307.6346] [INSPIRE].

[40] M. Cacciari, G.P. Salam and G. Soyez, *FastJet user manual*, *Eur. Phys. J.* **C 72** (2012) 1896 [arXiv:1111.6097] [INSPIRE].

[41] G. Cowan, K. Cranmer, E. Gross and O. Vitells, *Asymptotic formulae for likelihood-based tests of new physics*, *Eur. Phys. J.* **C 71** (2011) 1554 [*Erratum ibid.* **C 73** (2013) 2501] [arXiv:1007.1727] [INSPIRE].

[42] C. Brust, P. Maksimovic, A. Sady, P. Saraswat, M.T. Walters and Y. Xin, *Identifying boosted new physics with non-isolated leptons*, *JHEP* **04** (2015) 079 [arXiv:1410.0362] [INSPIRE].

[43] ATLAS collaboration, *Analysis of events with b-jets and a pair of leptons of the same charge in pp collisions at* $\sqrt{s} = 8$ *TeV with the ATLAS detector*, *JHEP* **10** (2015) 150 [arXiv:1504.04605] [INSPIRE].

[44] A. Hocker et al., *TMVA — toolkit for multivariate data analysis*, PoS(ACAT)040 [physics/0703039] [INSPIRE].

[45] ATLAS collaboration, *Search for new physics using events with b-jets and a pair of same charge leptons in* $3.2\,\text{fb}^{-1}$ *of pp collisions at* $\sqrt{s} = 13$ *TeV with the ATLAS detector*, ATLAS-CONF-2016-032, CERN, Geneva Switzerland (2016).

[46] R. Brun and F. Rademakers, *ROOT: an object oriented data analysis framework*, *Nucl. Instrum. Meth.* **A 389** (1997) 81 [INSPIRE].

[47] *BoCA: Boosted Collider Analysis webpage*, https://github.com/BoostedColliderAnalysis/BoCA, (2015).

[48] T. Plehn, M. Spannowsky, M. Takeuchi and D. Zerwas, *Stop reconstruction with tagged tops*, *JHEP* **10** (2010) 078 [arXiv:1006.2833] [INSPIRE].

[49] G. Kasieczka, T. Plehn, T. Schell, T. Strebler and G.P. Salam, *Resonance searches with an updated top tagger*, *JHEP* **06** (2015) 203 [arXiv:1503.05921] [INSPIRE].

[50] J. Gallicchio and M.D. Schwartz, *Seeing in color: jet superstructure*, *Phys. Rev. Lett.* **105** (2010) 022001 [arXiv:1001.5027] [INSPIRE].

JHEP01(2017)018